Evaluation of Inter-Modular Connection Behaviour Under Lateral Loads: An Experimental and Numerical Study

Heshachanaa Rajanayagam[1,2], Tharaka Gunawardena[3], Priyan Mendis[3], Keerthan Poologanathan[1], Perampalam Gatheeshgar[1,4], Madhushan Dissanayake[1], Marco Corradi[1,5].

[1]Department of Mechanical and Construction Engineering, Northumbria University, Newcastle upon Tyne, UK.
[2]ESS Modular, Crag Ave, Clondalkin Industrial Estate, Dublin 22, Ireland.
[3]Department of Infrastructure Engineering, University of Melbourne, Melbourne, Australia.
[4]School of Computing, Engineering and Digital Technologies, Teesside University, Middlesbrough, UK.
[5]Department of Engineering, University of Perugia, Perugia, Italy.

Abstract

This study focuses on a comprehensive investigation of the inter-modular connection shear behaviour under lateral load using theoretical, experimental, and numerical analyses. Initially, three design configurations of proposed inter-modular connection with varying bolt sizes and hole tolerances were tested in shear, and their load-deformation behaviours were studied. Finite element models were then developed in ANSYS and validated against the test results obtained from the experiments. The connections were identified as slip critical connections for serviceability design, as they tend to fail in slippage even at a very small lateral load. Further, evaluation of combined tension and shear effects on the connections confirmed that the failures were due to the combined effect not purely by shear, and therefore connections of this type should consider this as the most critical design check. Based on findings, this paper then describes a methodology for estimating the overall stiffness of inter-modular connections, such that those stiffness values can be employed in modelling the inter-modular connections as a link or spring type elements in the global model of modular buildings. This paper also presents recommendations and suggestions for future enhancement of inter-modular connection designs highlighting the shear slip behaviour and onsite installation constraints.

Keywords: *Modular buildings, Inter-modular connections, Experimental studies, Numerical studies*.

1. Introduction

Modular construction is the process of off-site manufacturing of modules or prefabricated units, which are then transferred to the site and readily assembled. Figure 1 shows a simplified graphical representation of a modular construction system. There are intense demands on housing production in various parts of the industrialised world. Modular Building Systems (MBS) are well recognised to have the ability to play a vital role in addressing the housing crisis at present. This contemporary building technique is a cost-effective and rapid construction solution, which can significantly impact the current housing market crisis. Despite a significant research gap in advanced techniques and structural performance, the uptake of MBS techniques is emerging more rapidly than on-site building practices in most developed countries (Sweden[1], UK[2], Australia [3], China and Canada[4]).

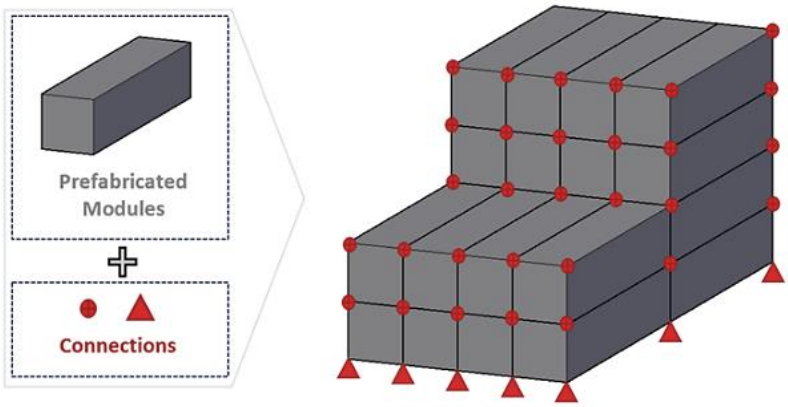

Figure 1: Graphical representation of MBS concept [5].

The use of modular construction possesses many advantages, which includes: enhanced speed of construction [4], higher quality management at the factory [2-5], work safety as reduced work required at high-altitudes [6]; rapid deployment of new technologies; construction not being affected by adverse weather[7]; decreased noise level and construction waste as on-site construction works are minimal [8]. In brief, modular and off-site manufactured building techniques eliminate most of the input from the construction site and effectively replace sluggish, unproductive site operations with quicker factory processes that are more effective. Despite such significant benefits, some critical challenges are experienced in the widespread adoption of modular construction technologies, most specifically in multi-storey structures [9]. Past studies have highlighted those difficulties in construction and installation [2], and reliability over critical connections [2-4] based on load transfer mechanism [4] and induced inter modular stresses [7] are some notable key factors influencing the reliability of MBS construction and its structural integrity. In that case, connections and bracings, most specifically intermodular connections (as shown in Figure 2) play a significant role in preserving the integrity of a module assembly by directly influencing the ultimate structural stability and robustness of MBS. In addition, inter-modular connections are crucial in resisting lateral loads and transferring them to stiffer vertical elements, especially in high-rise MBSs [10]. Previous research studies [10,11, 13] in relevant contexts have portrayed an overview of the structural performance and response of MBSs, for which a major limitation and challenge was acknowledged as designing and developing reliable, easily installable inter-modular connections.

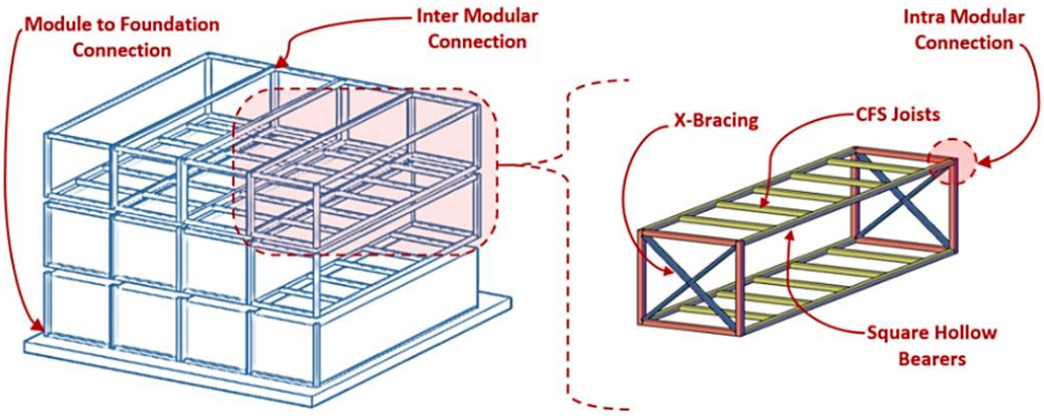

Figure 2: Graphical illustration of MBS connections and bracing.

Unlike in-situ reinforced-concrete (RC) and steel structures, MBSs construction requires more attention to detail in designing connections because of the need to accurately and conveniently connect multiple individual structural elements to form a modular unit, and modular units to develop a building as a whole [13] . In that context, an innovative connection has been proposed in this study, mainly targeting the inter-modular connections which forms the interface within modules. In MBSs, the inter-modular connections provide Horizontal Connectivity (HC), and/or Vertical Connectivity (VC) as presented in Figure 3.

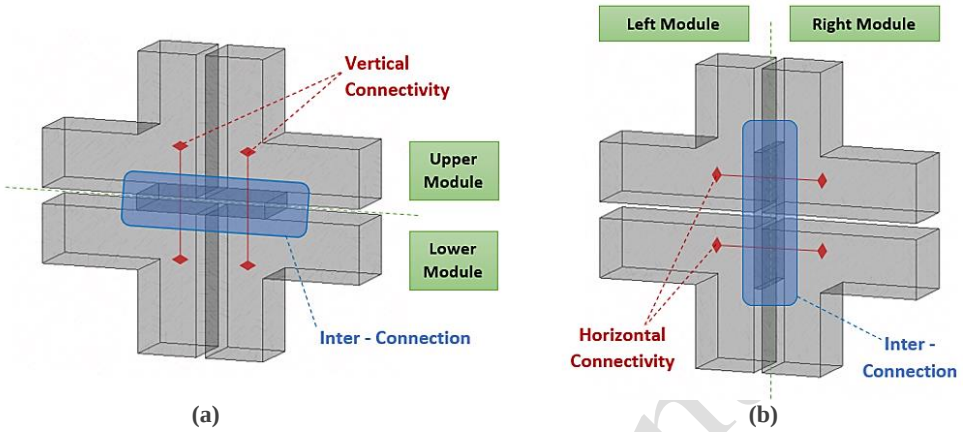

Figure 3: Vertical (a), and horizontal (b) connectivity of inter-modular connections [5].

Most common inter-modular MBS connections include bolted plate or site welded details; Figure 4 (a-c) illustrates some examples of currently employed steel connections. However, these currently used inter-modular connections have several disadvantages in terms of application and installation [4, 8].

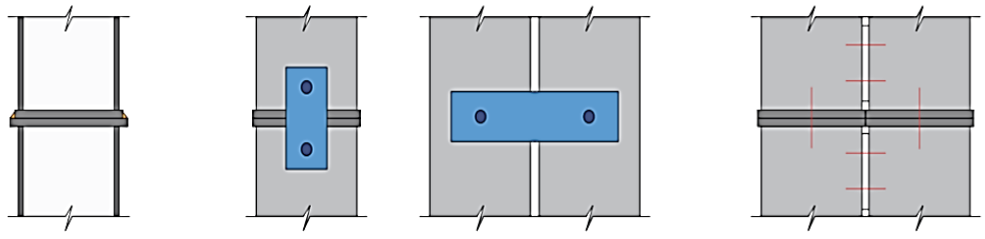

(a) Site welded plates [8-10], (b) Tie plates [11-12], (c) Bolted side plate [19] and end plate [20].

Figure 4: Most typical inter-modular connections used in the industry.

In the case of intermodular connections, modular units are generally linked in their corners by mechanical fasteners (both vertically and horizontally, Figure 4c) in the conventional design of MBSs in order to ensure both vertical and lateral stability of the structure. A potential downside in the use of these mechanical fasteners is accidental teardown under abnormal loading circumstances. Another limitation in the use of these types of joints is the stress concentrations at the fastening points if not properly designed. This can lead to tearing of these connections and initiate unfavourable local failures threatening the structure's overall stability. In that case, it is essential to define MBSs connection systems' ability to resist the applied load, and on the other hand, limit the potential for over-design due to limited understanding. Further, the inter-modular connections must provide suitable tolerances to allow positioning of the modules on site. In that case, the on-site welded details as illustrated in Figure 4a, unlike bolted connections, will enable increased flexibility in the positioning of the modules. The

site welding process, however, adds another trade into the site work, which is undesirable if the priority is to optimise construction cost and speed while increasing the work quality. In addition, comparatively simple joints or assembling points might become complicated if connecting points of modules are required in 3 directions while providing access for installation to the relevant point on-site [15]. Past studies and research [4-14,21] have proven that a promising improvement in inter-modular MBS connection design with a more detailed understanding of its behaviour to avoid overdesign is inevitable. Hence this study focuses on proposing a new intermodular connection design and identifying the role and behaviour of proposed intermodular connections in MBS lateral load resistance system performance with the help of theoretical, experimental and comprehensive 3D Finite Element Analysis (FEA). The 3D FEA was conducted using ANSYS [22], and an advanced contactless measurement system ARAMIS [23] with high-definition photogrammetry was used for the experiment. Based on the simulation and test results, a methodology was proposed for estimating the overall rigidity of intermodular connections, such that these rigidity or stiffness values can be employed in modelling the connection as a link or spring element in a global model of MBSs. In addition to that, this paper also presents the critical failure criteria of the intermodular connection using a validated finite element model and suggests appropriate strategies to optimize the connection design further for strength and serviceability requirements.

2. Inter-modular Connection

2.1. Connection Detail

Based on the understanding of the knowledge gap and considering the challenges faced in the modular construction industry, a novel connection design was proposed. The detailed design and 3D view of the connection proposed are illustrated in Figures 5 and 6. The 4 Square Hollow Sections (SHS) represent the 4 corner columns of the modules which get connected at one joint.

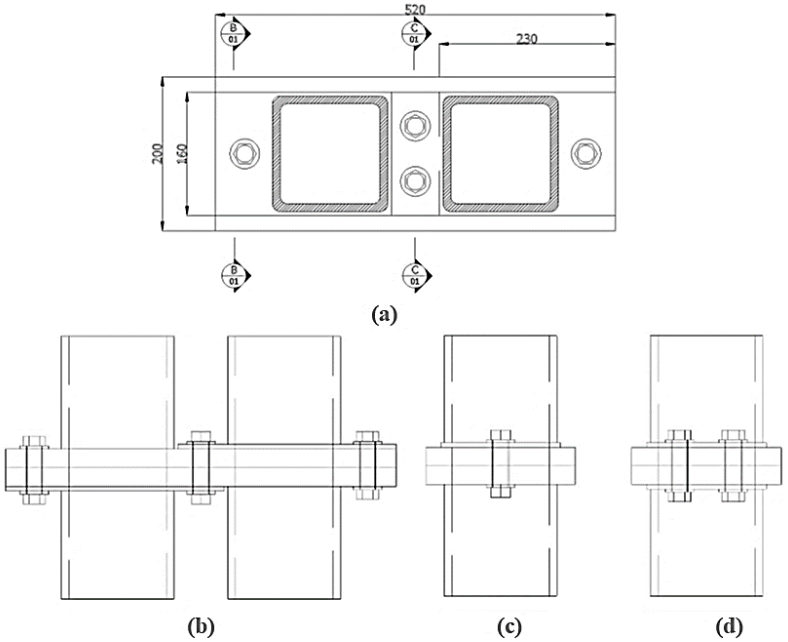

Figure 5: Detail of proposed module to module connection (a) top view, (b) front view and cross-sectional views (c) section B-B and (d) section C-C.

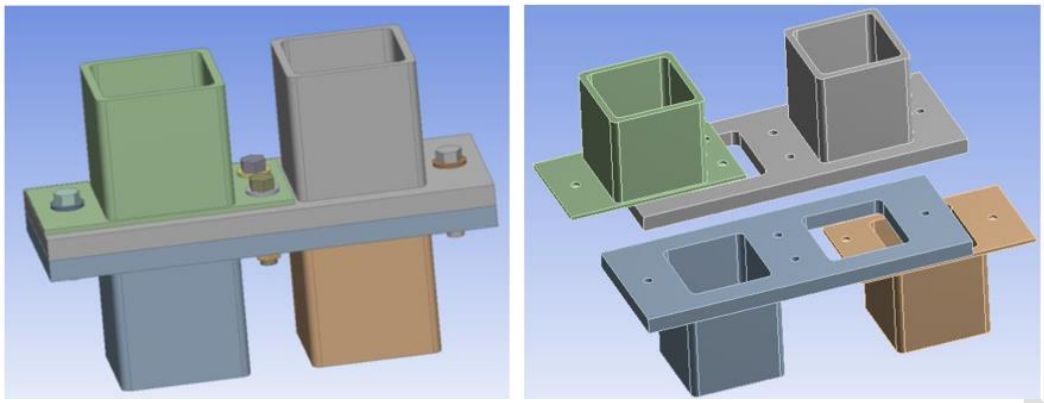

(a) (b)

Figure 6: 3D model of proposed inter-modular connection (a); exploded view (b).

In order to satisfy the performance requirements of a corner supported MBS, the connection is designed to resist and to transfer both horizontal and vertical loads. As illustrated in Figure 6, the proposed connection unit, both vertically and horizontally, will connect four neighbouring modules. Three different connection design parameters were considered for the experiment and the FEM validation. The varying parameters were the size of bolts (bolt diameter), and shape and size (diameter) of bolt holes, as illustrated in Table 1 and Figure 7.

Table 1: Details of connection design (C1-C3).

Connection type	Bolt diameter (mm)	Bolt type and hole diameter (mm)
C1	12	Round, 14
C2	16	Round, 18
C3	16	Slotted, 18

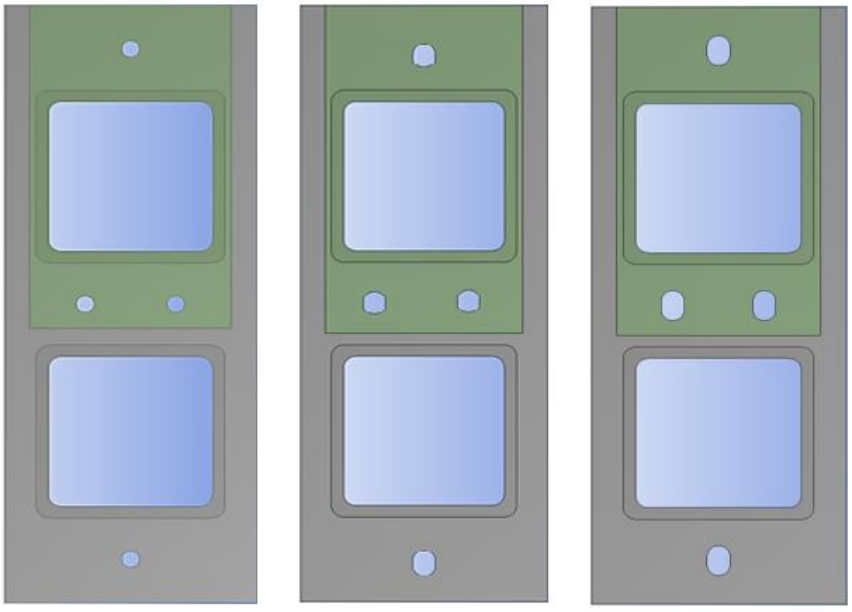

(a) (b) (c)

Figure 7: Three different connection design configurations (a) C1 with 14 mm round bolt hole, (b) C2 with 18 mm round bolt hole, and (c) C3 with 18 mm slotted bolt hole with slot size of 26 mm.

2.2. Theoretical Study on Connection Capacity

Australian steel design standard AS 4100 [24] and supporting guidelines [25] were used for the calculation of nominal shear capacity and slip resistance of the proposed connection design. The calculation elaborated in this paper is only for design of connection C1, where a similar procedure was adopted for design of connection C2 and C3.

2.2.1. Calculation of Nominal Shear Capacity

Based on the guidance provided under AS 4100 [24] clause 9.3.2, the nominal shear capacity of the proposed connection was calculated. As illustrated in Figure 8(a), the 2 bolts in the middle will cover 3 shear planes each, and the other 2 bolts in the corners will cover 2 shear planes each when this connection is applied in a real modular building. However, as discussed in detail later in section 3, the experimental setup was planned in a way to apply a shearing force through the centre of the overall connection using a vertical load cell. This setup allowed columns to freely move under the applied load. Since only one 25 mm thick plate of the connection was connected to the load cell, all bolts will lie at the common interface of the two 25 mm thick plates in a single shear plane as shown in Figure 8(b). Hence, only one shear plane was considered for the purpose of this study and for the design of connection and its three design variations (C1, C2 and C3).

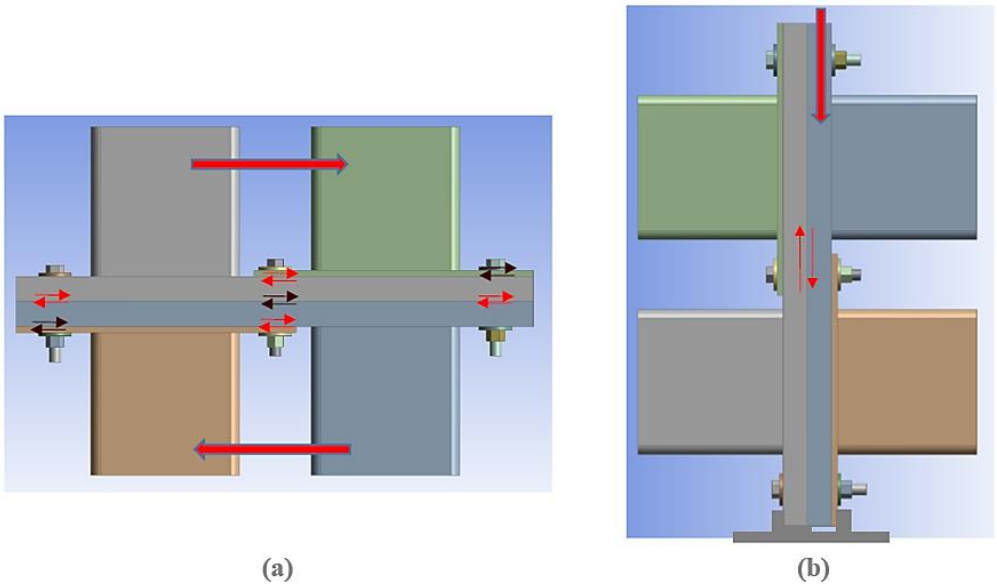

Figure 8: Shear planes in the proposed connection (a) for axially loaded columns; (b) for the experimental setup and finite element analysis

The shear capacity and preload limit for the connection were calculated based on checks for the shear failure of bolts, crushing or bearing and tear-out failure of ply.

In this study, the shear capacity of a single bolt (V_f) was calculated using Eq. (1), where the equation is used only to interpret the capacity of the connection as per the experimental setup. In order to obtain the design shear capacity of the proposed connection as per AS 4100 [24], the output value from Eq. (1) should get multiplied by a capacity reduction factor of 0.8.

$$V_f = 0.62\, k_r\, f_{uf}\, n_x\, A_0 \quad (1)$$

Where k_r is the reduction factor for the length of the bolt (takes a value of 1.0 for non-lap connections); f_{uf} is the tensile strength of the bolt; n_x is the number of shear planes (unthreaded region); A_0 is the cross-sectional area of bolt shank (considering no shear planes in the threaded region). Accordingly, the shear capacity of an individual bolt and all four bolts together will be 56.1 kN and 224.4 kN, respectively. The bearing capacity of the ply (V_b) was calculated using Eq. (2),

$$V_b = 3.2\, t_p\, d_f\, f_{up} \quad (2)$$

Where t_p is the thickness of the ply; f_{up} is the ultimate tensile strength of the ply; d_f is the bolt diameter. Considering 6 mm thick ply as the critical ply thickness for bearing failure, the maximum bearing capacity of the ply under the preload of an individual bolt was calculated using Eq. (3), and it was found that all the bolts can be preloaded at maximum to (= 3.2 × 6 mm × 12 mm × 450 MPa) 103.7 kN. Further, the connection was checked against tear-out failure (V_p) using Eq. 3 as follows,

$$V_p = a_e\, t_p\, f_{up} \quad (3)$$

Where a_e is the minimum distance from the centre of the hole in the direction of the bearing load to the ply edge. Based on Eq. (3), the tear-out capacity (V_p) near an individual bolt and the complete C1 connection was calculated as (= 35 mm × 6 mm × 450 MPa) 94.5 kN and (= 4 × 94.5 kN) 378 kN respectively. Therefore, considering all failure criteria, the shear capacity of the overall C1 type connection was deduced as equal to the shear capacity of bolts which is 224.4 kN.

2.2.2. Calculation of Slip Resistance

The proposed connection was considered a 'slip critical' connection in this study due to its geometric position in a modular building structure and the load types the connection could undergo during a seismic event. According to AS 4100 [24], slip failure of a connection is addressed as serviceability limit criterion, and the slip resistance (V_{sf}) is calculated as in Eq. (4)

$$V_{sf} = \mu\, n_{ei}\, N_{ti}\, k_b \quad (4)$$

Where μ is the coefficient of friction between plies; n_{ei} is the number of shear planes; N_{ti} is the minimum preload on bolts applied during installation (31.8 kN - AJAX Fastener Handbook [26]); k_b is the factor for the type of hole used in the connection (1.0 for standard holes, 0.85 for oversize holes and short slots and 0.70 for long slotted holes). Using Eq. (4) the shear slip resistance for an individual bolt and the entire C1 connection was obtained as (= 0.2 × 1 × 31.8 kN × 1) 6.36 kN and (= 4 × 6.36 kN) 25.44 kN respectively.

The summary of shear capacity, preload limit (per bolt) and slip capacity calculated based on the Eq. (1) - (4) for all three types of connections is provided in Table 2.

Table 2: Summary of the capacity of three types of connections proposed.

Connection design	Shear capacity (kN)	Bolt pre-tension limit (kN per bolt)	Slip capacity (kN)
C1	224.4	103.7	25.4
C2	398.9	138.2	47.4
C3	398.9	138.2	40.3

3. Experimental Study

3.1. Test Setup and Instrumentation

The laboratory experiment was carried out in order to understand the shear-slip behaviour of the proposed connection subjected to later load. As illustrated in Figure 9, the connection specimens were mounted onto a supporting steel table and was placed under a vertical load cell with a maximum loading capacity of 500 kN. The setup was arranged in a way to induce a shear force in the connection equivalent to the vertical compressive load from the load cell. The base support attached to the steel table prevents one plate from sliding down while allowing the other to move freely (see Figure 10). Another identical block is placed at the top of the specimen, allowing the opposite plates to move freely while restraining the other from moving.

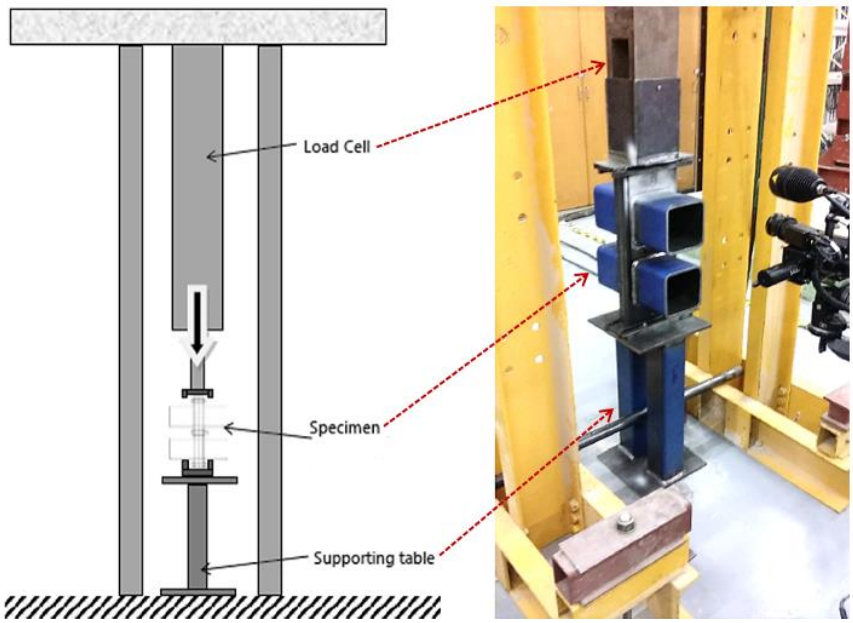

Figure 9: Schematic diagram of the experimental setup (left); specimen setup prior to loading (right).

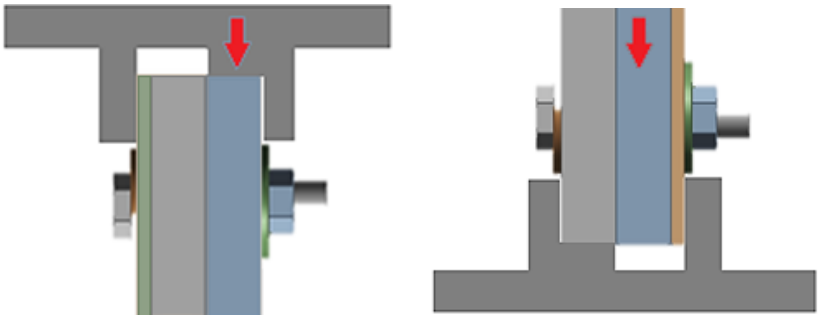

Figure 10: Schematic detailed close-up view of specimen, base attached to the supporting block (left); top attached to the load cell block (right).

An advanced contactless measurement system called ARAMIS [23] which gauges strains in both 2D and 3D environments with high-definition photogrammetry was employed to carry out the proposed experiment. The adoption of this system was mainly to obtain accurate strain values to validate the finite element models without any hassle from attaching strain gauges and other strain measurement kits to the specimen. The specimens were placed under the load cell; the target area was sprayed with white matte paint to provide a contrasting and anti-reflective surface and was kept focused by the ARAMIS camera, as shown in Figure 11. The lighting around the specimen's target region was meticulously adjusted to ensure that the image on display was as sharp and clean as possible. The loading and displacement values were directly obtained from the load cell's data logger. 0.1 mm/min rate displacement-based load was applied as the vertical load, since the experiment was intended to be performed at a slow phased loading rate.

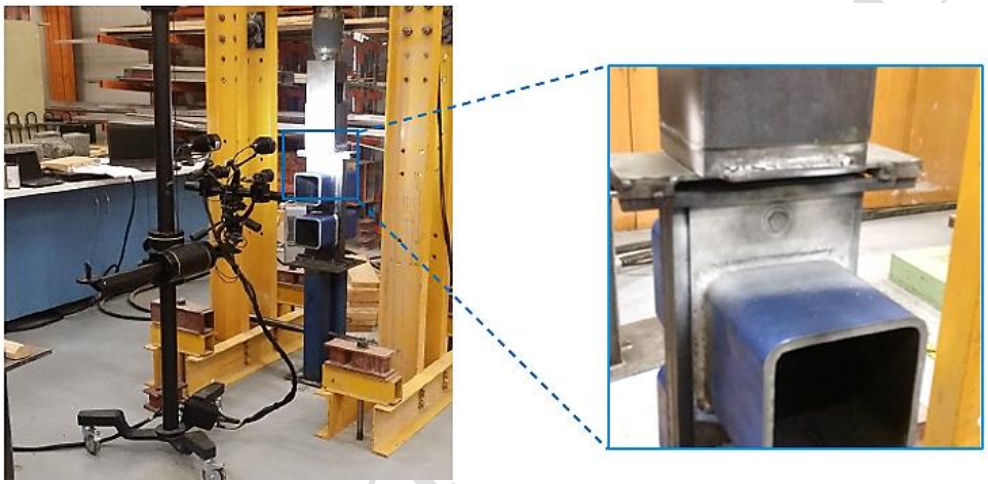

Figure 11: ARAMIS camera focused on the targeted area painted for strain measurement.

4. Finite Element Modelling and Validation

4.1. Design and Methodology

This section provides the details of the extensive FE modelling carried out in this study using ANSYS software package [22] to investigate the structural behaviour of the module-to-module steel connection when the lateral load is applied. The experimental setup of the inter-modular connections were closely followed during the implementation of the FE models. Three separate numerical models were created in ANSYS using the transient structural module to simulate three connection types: C1, C2 and C3 where the size of bolts, and both size and type of bolt holes were the same as those used for the experiment (as per Table 1). Further details of the bolts, nuts and bolt holes considered for each of the finite element models of the connection types are given in Table 3. The bolt and nut details and fastening specifications including pre-tension values were determined using the AJAX Fastener Handbook [26]. During the 3D model development, different components of each connection were created and meshed. Then, material properties were assigned to them, and they were assembled. After that, each connection was given appropriate loading and boundary conditions, and suitable contact interactions were defined

between different components in contact. Figure 12 shows the 3D FE model created in ANSYS to simulate the connection and its different components.

Table 3: Details of bolts, nuts and bolt holes considered in the FE modelling of connections C1-C3.

Parameters	Values used for each connection type		
	C1	C2	C3
Bolt diameter (mm)	12.0	16.0	16.0
Hole type and diameter (mm)	14.0, round	18.0, round	18.0, slotted
Slot size (mm)	N/A	N/A	26.0
Pitch of threads (mm)	1.75	2.0	2.0
Bolt head thickness (mm)	7.5	10.0	10.0
Bolt head width across flats (mm)	18.0	24.0	24.0
Bolt head width across corners (mm)	20.03	26.75	26.75
Nut thickness (mm)	10.58	14.45	14.45
Nut width across flats (mm)	18.0	24.0	24.0
Nut width across corners (mm)	20.03	26.75	26.75
Bolt pre-tension	31.8 kN	59.2 kN	59.2 kN

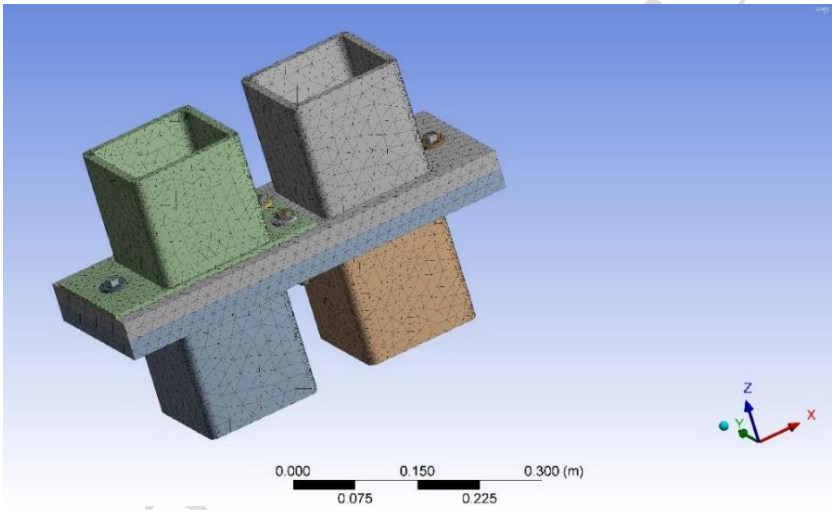

Figure 12: 3D ANSYS model of the module-to-module connection.

When defining the material properties in the FE models, yield strength of 350 MPa [27] was assigned to four square hollow section columns and 25 mm and 6 mm thick steel plates. Grade 8.8 bolts were modelled with a yield strength of 660 MPa [27]. A minimum tensile strength of 800 MPa was considered for the bolts [26]. The Young's modulus and the shear modulus of steel were taken as 200 GPa and 80 GPa, respectively.

The element type provided in ANSYS as 'Solid 185' with an elastoplastic stress-strain behaviour was used to model the structural steel components of the finite element models. The mesh sizes were selected to be close to 1.0 for all components controlled by the length-to-width aspect ratios. More finer mesh sizes were adopted around the bolt holes in order to transfer the stress from the bolt to the plates and to detail the deformation of bolt holes. The bolt pretension loads were generated in the developed FE models with pretension element in the middle section of the meshed bolt shank. The bolt pretension loads of 31.8 kN and 59.2 kN [26] is applied for bolt body and force is applied to the nut surface which

indicated the amount of force required to tight the nut. All steel-steel contact surfaces were defined as frictional contacts with a frictional coefficient of 0.2. Further, the threaded region of all bolts were defined as bolt thread contacts with properties as given in Table 3.

When applied in a real building, both wind and seismic forces would transfer as shear forces through the inter-modular connection. Therefore, a monotonic lateral load was applied to the connection (vertical load to the test setup) to examine its response under these loading conditions. The boundary conditions of the model were applied to reflect the experimental conditions as closely as possible. One 25 mm thick plate was restrained at its two ends to lateral forces, while the other 25 mm thick plate was set free to move when a lateral load was applied. In addition, the bolts were assigned pre-tension forces, which are equal to the values given in Table 3. Finally, a static load was applied to one edge of the 25 mm thick plate, which is free to move against lateral loads. Upon completion of the 3D FE models of modular connections, a nonlinear analysis was performed. The analysis results were then compared with the experimental results to assess the accuracy of the developed numerical models. The test and FE load-deformation responses were compared as illustrated in Figure 13 for all three connection types. The shear deformation of the steel bolt was calculated by sum of deformation at 2 mid points of bolt shank as illustrated in Figure 14. Three different stages can be identified from the load-deformation curves of each connection, and the comparisons show that the numerical load-deformation response closely followed the experimental response in all three stages. Figure 15 provides the expected detailed behaviour of a clamping bolt according to Gorenc et al. [28], which is similar to those used in the test specimens.

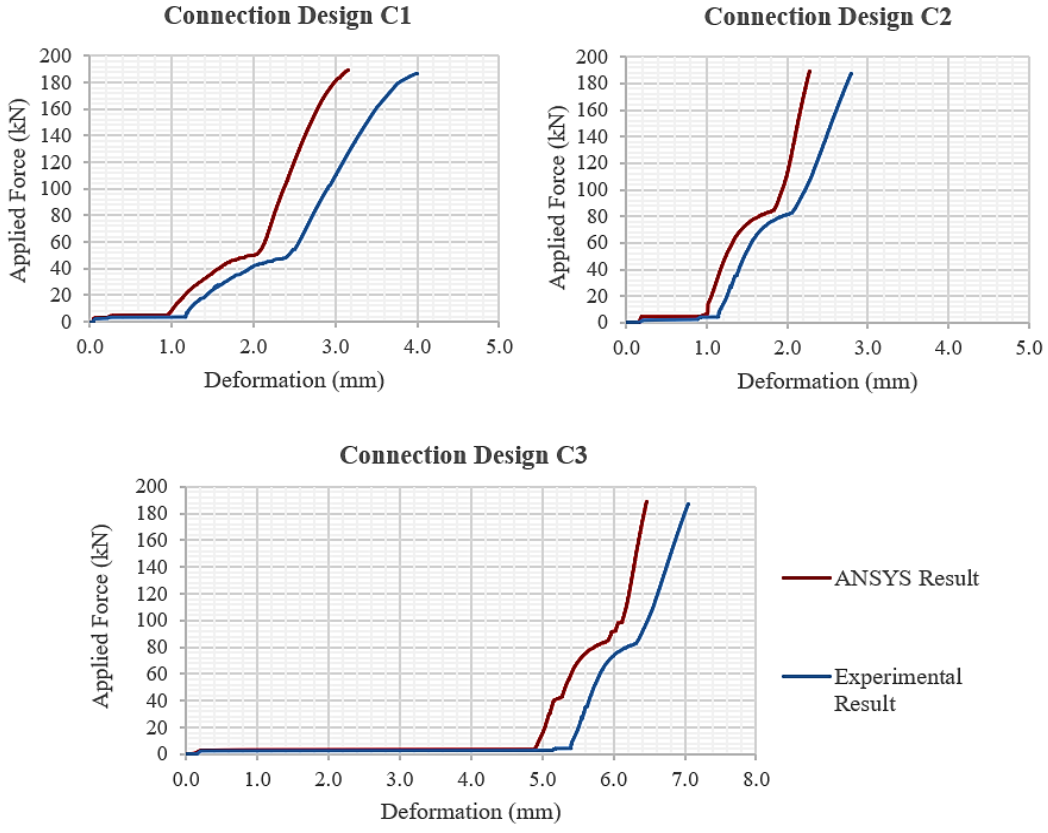

Figure 13: Comparison of load-deformation responses of experiment and ANSYS model for the connection C1-C3.

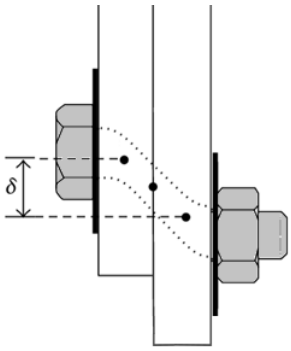

Figure 14: Deformation of single bolt connection.

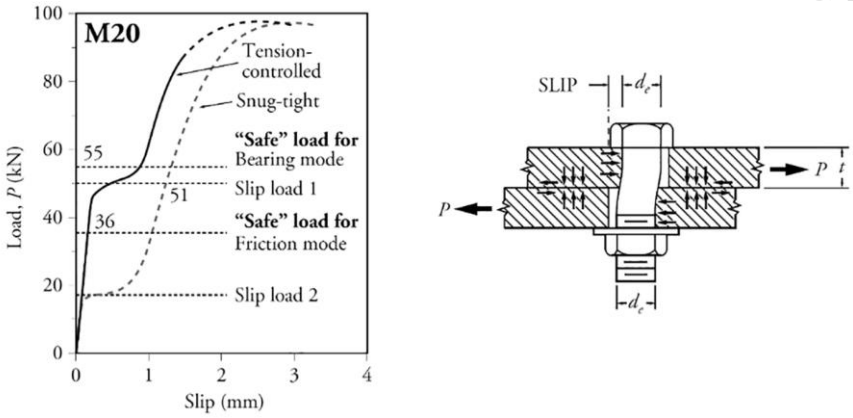

Figure 15: Expected behaviour of bolts under combined bearing and shear stresses [28].

A rapid deformation is observed at the beginning of the curves as a result of the initial slip of the connections. The tolerance between the bolt hole and bolt allows for this initial slip which is about 1 mm for connection types C1 and C2 and is equal to an approximately higher value of 5 mm for connection type C3 with slotted holes. The irregularities of plate geometries and the deviations of bolt orientation from its centre axis in the tested connections could be the reasons for slight deviations observed between the experimental and numerical curves. When at least one bolt has reached the edge of its bolt hole under lateral loading, the overall stiffness of the connection begins to increase. The settled bolt would contribute fully to the resistance of the connection against the lateral loading. Gradually other bolts also would follow this path and result in contributing to the overall stiffness of the connection in full capacity. The second stage of the load-deformation response corresponds to this phenomenon. The overall slip resistances of each connection can be identified from the loads equivalent to the end of this second stage and are given in Table 4. Finally, all the components in the connection act together in resisting the lateral load in the third stage of the load-deformation curve. The bolts begin to show both shear and bearing deformations in this stage. The stiffness exhibited in this stage of the curve corresponds to the lateral stiffness of the overall connection. Table 4 compares the test slip resistances and analytical slip resistances obtained from ANSYS for all three connections. The test-to-FE slip resistance ratios given in Table 4 confirm that the developed 3D FE models of inter-modular connections can predict their slip resistance with good accuracy.

Table 4: Comparison of experimental and ANSYS slip resistances of the connections.

Connection Type	Slip resistance (kN)		Test/ANSYS slip resistance ratio
	Test	ANSYS	
C1	51.8	48.5	1.07
C2	84.0	81.5	1.03
C3	83.5	81.0	1.03

4.2. Strain Measurements

The contactless strain measurements that were taken with the aid of the ARAMIS system is compared here against the results from the ANSYS model. To increase accuracy of the comparison process, five nodes were selected from the ARAMIS results where the measurements were clear for the total duration of the experiment. The five points that were marked to measure the strain results through the duration of the test is illustrated in Figure 16. The marked points A, B, C, D and E were at similar locations to the stage points 0, 1, 2, 3 and 4 from the ARAMIS strain measurement. A sample strain results plot from ARAMIS for a time at the initial part of the loading is illustrated in Figure 17. The results obtained from this comparison as a part of validating the developed model with laboratory test data were satisfactory with the coefficients of determination ranging from 0.61 to 0.99. Hence the developed and validated ANSYS models were proved to be conservative in comparison with the experimental outputs.

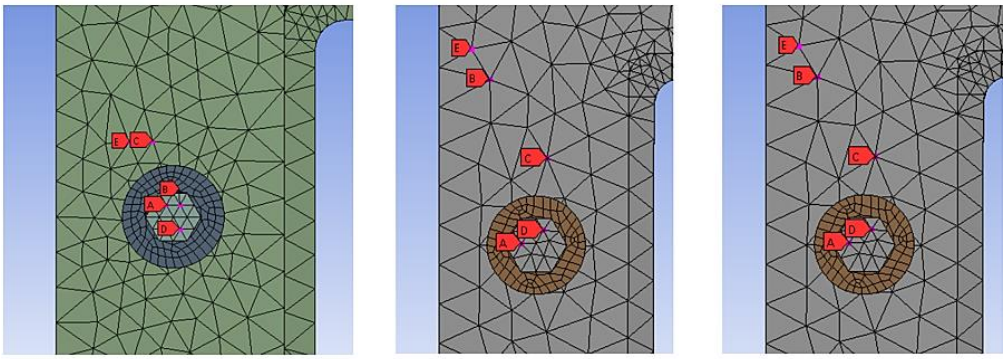

Figure 16: Five points (A-E) marked on the ANSYS models to measure von Mises strains for connection designs (C1-C3).

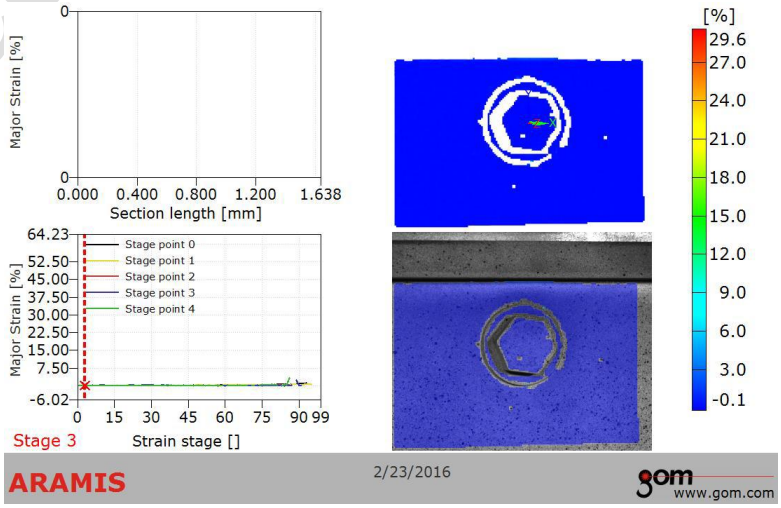

Figure 17: A sample strain results plot from ARAMIS for a time at the initial part of the loading.

5. Failure Modes and Design Criteria

Generally, bolted connections fail due to bearing, tension or shear of the bolts, tear-out of bolt holes, bearing of the plates, or a combination of all these. Therefore, in order to establish a specific, detailed design procedure for the proposed connection, the validated finite element models were further critically evaluated to identify the most critical failure modes bolts 1-4 (illustrated in Figure 18) under shear (lateral load).

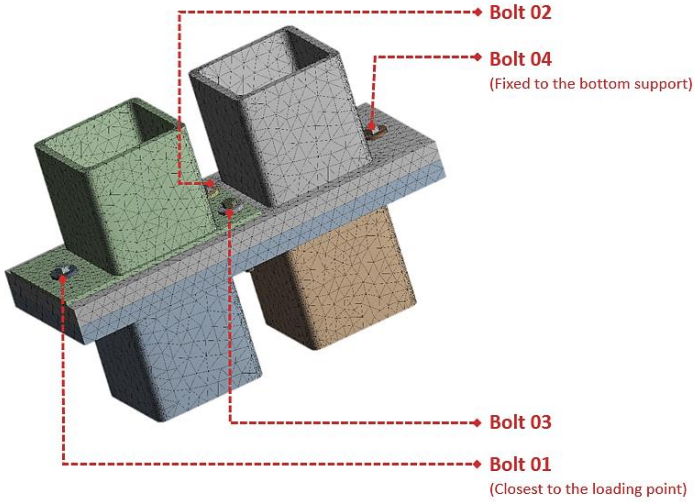

Figure 18: Designated bolt numbers (1-4) in the connection specimen.

5.1. Stress and Strain Behaviour of Bolts

The proposed connection is a slip critical connection where initially the friction in the bolts resists the applied shear force until it reaches the slip stage, after which, on the bolts against the plies it will be resisted as a bearing force. The overall failure of the bolts in the connection was studied using Distortion Energy Theory (DET), according to which the knowledge of von Mises stresses can help to understand the behaviour of the overall connection. Figure 19 illustrates the results obtained from the finite element analysis using ANSYS for the equivalent (von Mises) stresses development through the loading history for the bolts in connections C1 to C3.

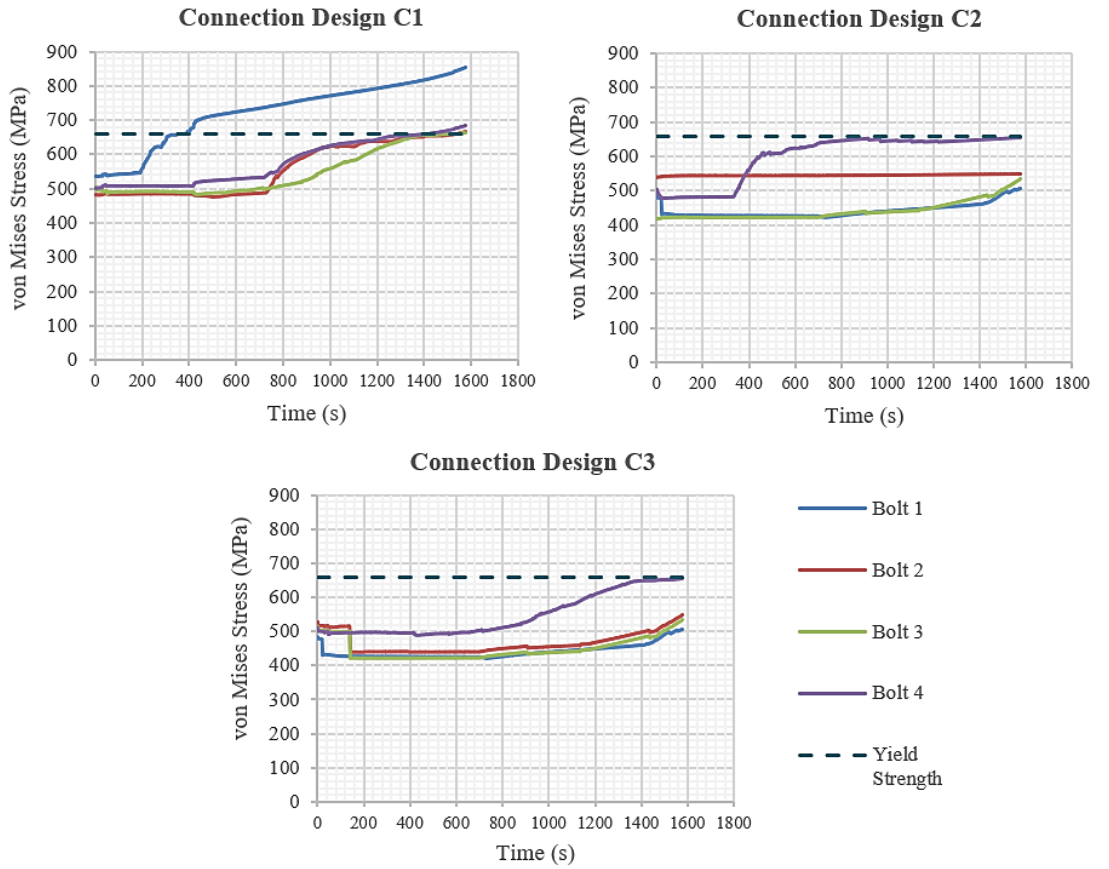

Figure 19: Equivalent (von Mises) stress development in the bolts of connection designs (C1-C3) through the loading history.

According to Figure 19, solely in C1 connection appears to be yielding through bolt 1 at first, then the following 3 bolts as the loading history progresses. Unlike in connection C1, in the connections, C2 and C3, Bolt 4 which is nearest to the bottom support, has developed the largest strains even though neither of those bolts have yielded. Further, to pinpoint the specific mode of failure and to understand whether the yielding occurs due to specific one action or a combined effect, the shear stresses, principal stresses and combined effect of tension and shear were evaluated in detail for all three types of connections.

5.1.1. Evaluation of Shear Stresses

The generated graphs presented in Figure 20 describes the shear stress generated against strains in each bolt of C1-C3 connection designs. The graphs indicate an equivalent gradient of liner shear stress-strain relationship with an approximate value of 76.9 GPa, which is equal to the shear modulus of the material. Hence, it is evident that generated strains and stresses vary from one bolt to the other, none of the connections faces pure shear failure, and shear stress generated in the connection is not born equally by all four bolts. Design codes in general, would assume that all bolts bear an equal degree of shear force. However, it should be noted that according to AISC (1980) shear stress experienced by each bolt in a bolted connection vary with the distance from where the load is applied and the distance within the bolts of the connection. Figure 21 presents the graphs of shear stress plotted against the bolt deformation in load direction. The initial slip of 1 mm in connection C1 and C2, and 5 mm in connection C3 due to

bolt clearance and development of shear stress in bolts immediately after the slip is clearly captured in the graphs.

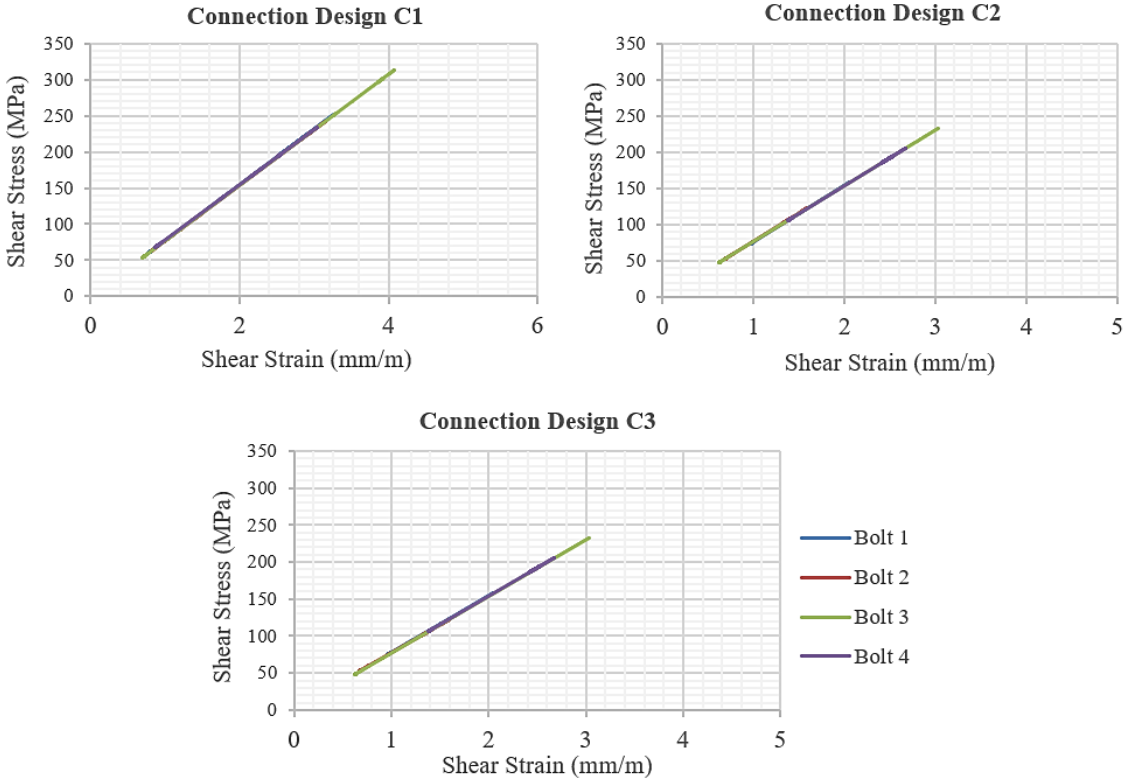

Figure 20: Shear stress vs shear strain relationship for the bolts in connection designs (C1-C3).

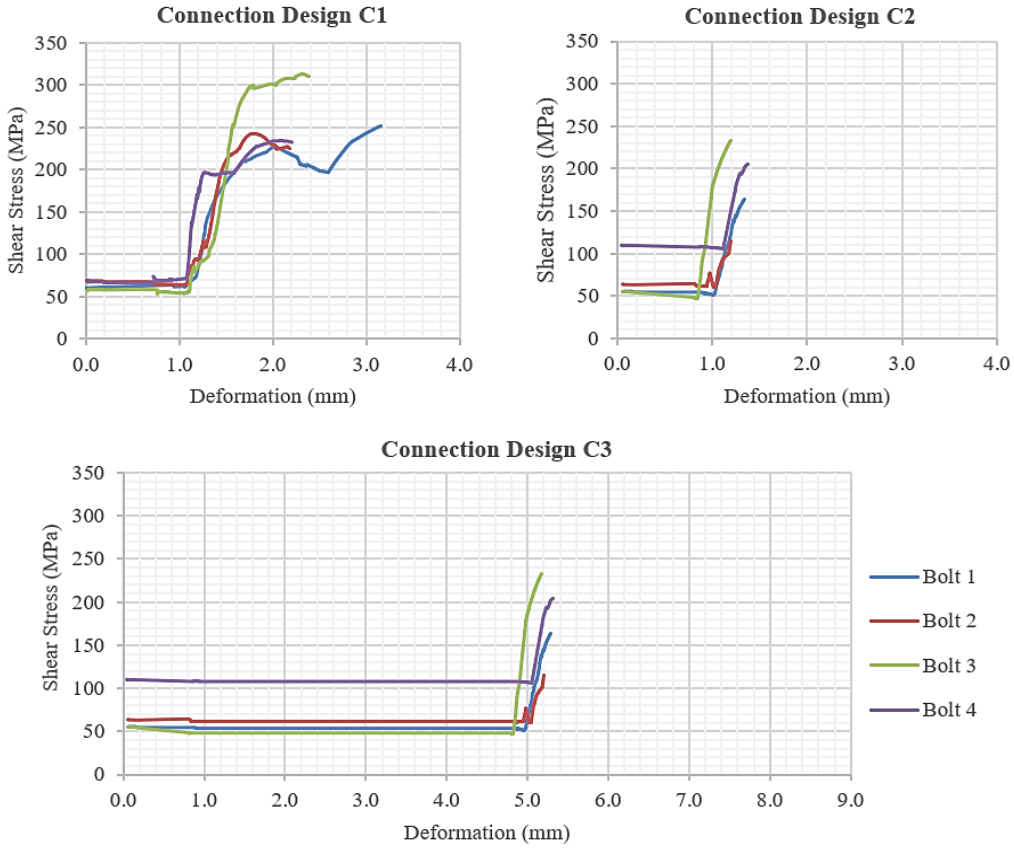

Figure 21: Shear stress vs deformation of the applied load for the bolts in connection designs (C1-C3).

The reason for shear values not starting from zero is because the specimens were kept vertical under the load cell and before the external load gets applied from load cell the connections' self-weight itself adds shear load on the bolts. As a result, Bolt 4 (furthest from the load applied point and closest to the bottom support) has the largest shear stress at the beginning as it takes the largest portion of the connection's self-weight. Similar to Figure 21, The graph (Figure 22) by Kulak et al. [29] illustrates a detailed shear stress vs deformation relationship for a steel bolt which highlights the shear-slip deformation behaviour and yielding through the nonlinearity with evident change in the gradient.

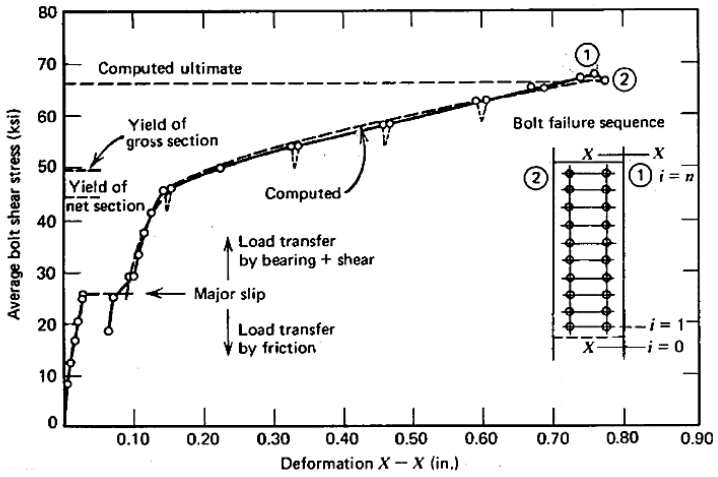

Figure 22: Experimental and theoretical results for shear stress vs deformation relationship for a slip critical bolt connection [29].

5.1.2. Evaluation of Principal Stresses

In order to study the failure modes of bolts in the connection, the stress vs strain relationships were analysed for connection designs C1-C3 (shown in Figure 23).

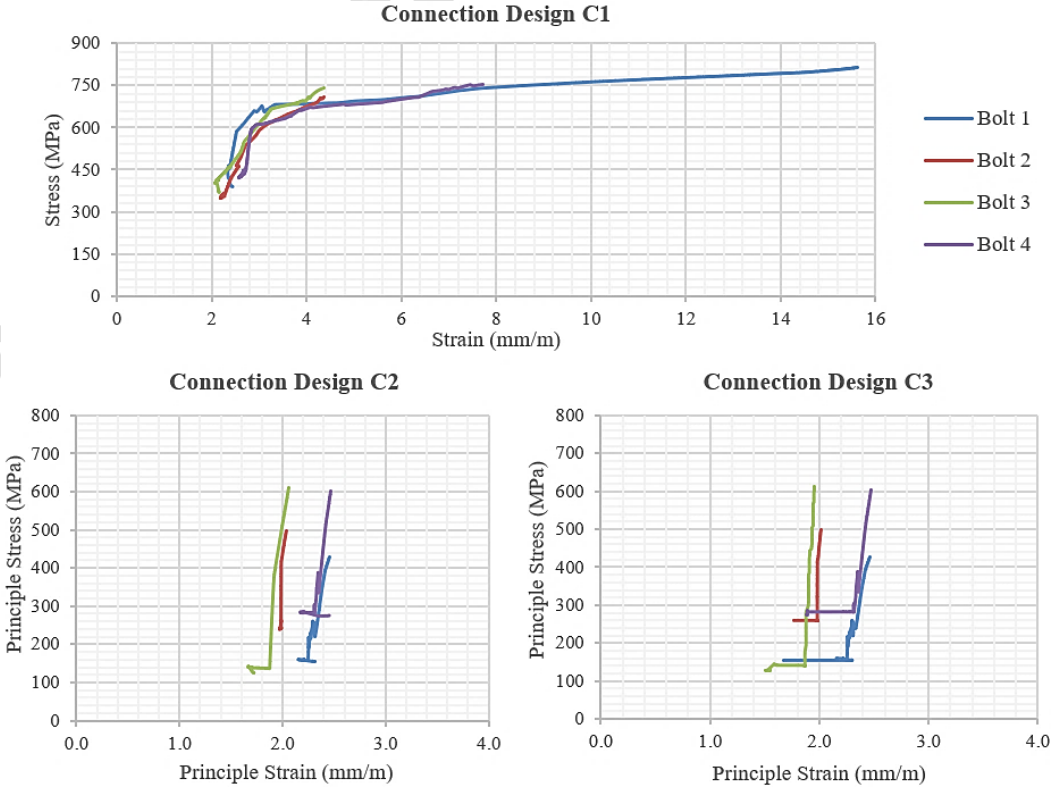

Figure 23: Principal stress vs strain relationship for each bolt in connection designs (C1-C3).

An evident nonlinearity for all four bolts (especially Bolts 1 and 4) can be observed in the principal stresses for connection C1, unlike in C2 and C3. Even though Maximum Principal Stress Theory (MPST) is not an ideal assessment for yielding behaviour of bolted connections, it clearly indicates development of significant axial stresses in all 4 bolts of the 3 connection designs.

5.1.3. Evaluation of the Combined Effects of Shear and Tension

The combined tension and shear effect can be considered critical for the connections because of the frequent and early slip failures in their loading histories. According to AS 4100 [24], the interaction relationship between tension shear for bolt connection can be expressed as in Eq. (5). The combined effect of tension and shear against their capacity calculated using Eq. (5) are presented in Figure 24.

$$\left(\frac{V_f^*}{\emptyset V_f}\right)^2 + \left(\frac{N_{tf}^*}{\emptyset N_{tf}}\right)^2 \leq 1 \quad (5)$$

Where, V_f^* is the design shear force of the bolt; V_f is the nominal shear capacity of the bolt; N_{tf}^* is the design tensile force of the bolt; N_{tf} is the nominal tensile capacity of the bolt; and $\emptyset$ is 0.8 - the capacity reduction factor as per Table 3.4 of AS 4100 [24].

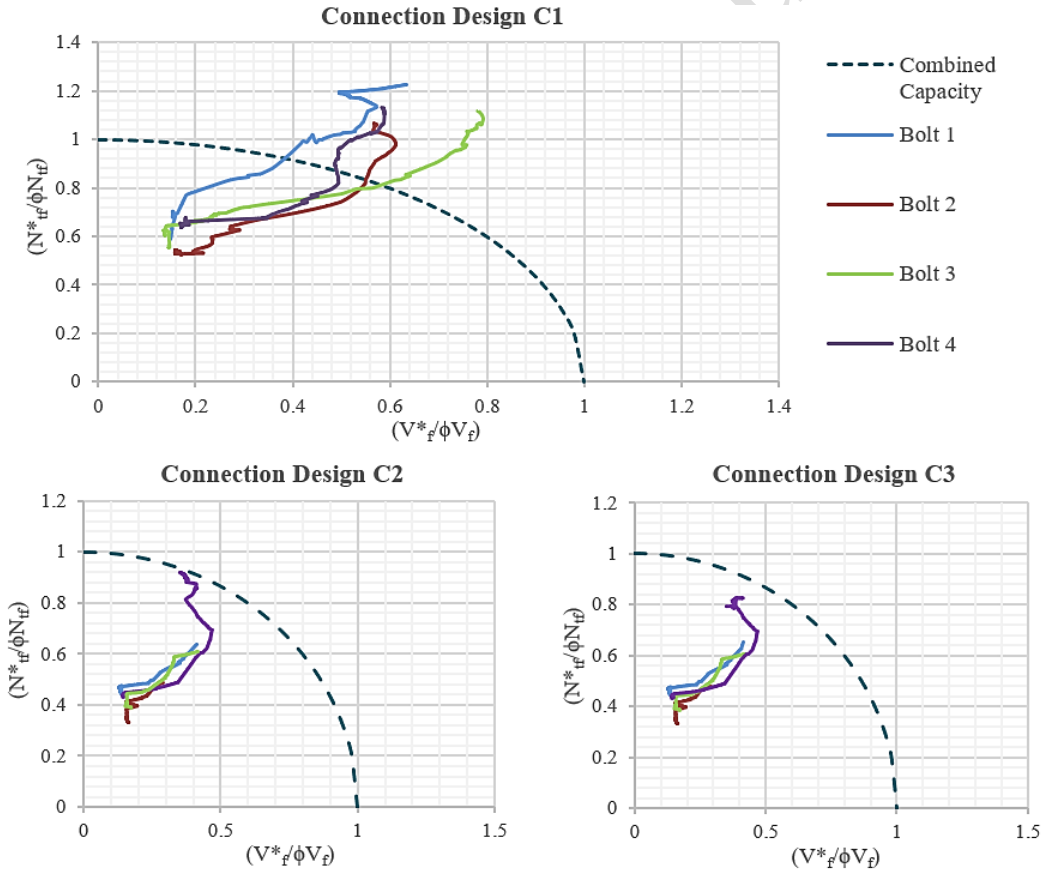

Figure 24: Combined shear-tension interaction diagram for connection design C1-C3.

Considering the magnitude of the applied loads, it can be noted that none of the bolts in connections C2 and C3 undergo yielding, and all 4 bolts in connection C1 have yielded through combined tension and shear (Figure 24). The failure pattern of bolts in connection C1 is further illustrated through images from ANSYS analysis and presented in Figures 25 and 26. From the figures, it also can be concluded

that these bolts have failed due to both shear and the axial stresses caused by bearing (within the inside surface of the bolt hole), and the failure mode is a combination of tension and shear.

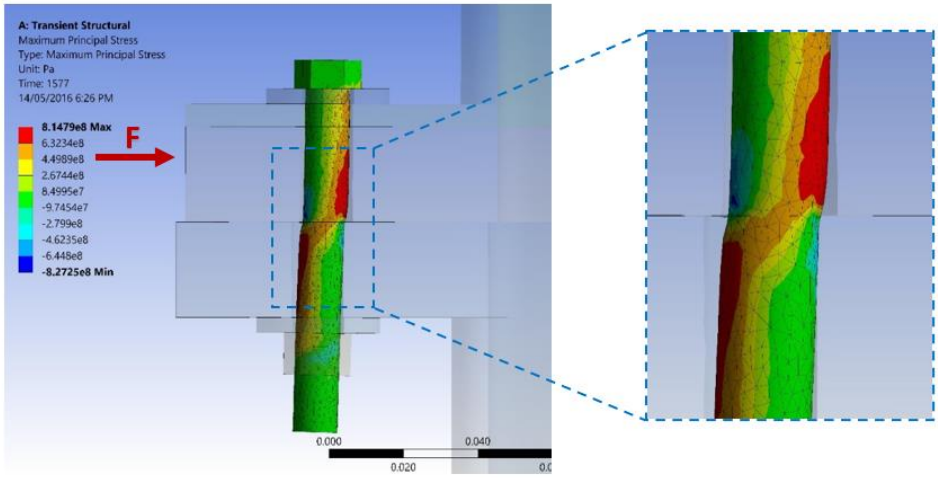

Figure 25: The failure zone of Connection design C1, Bolt 1.

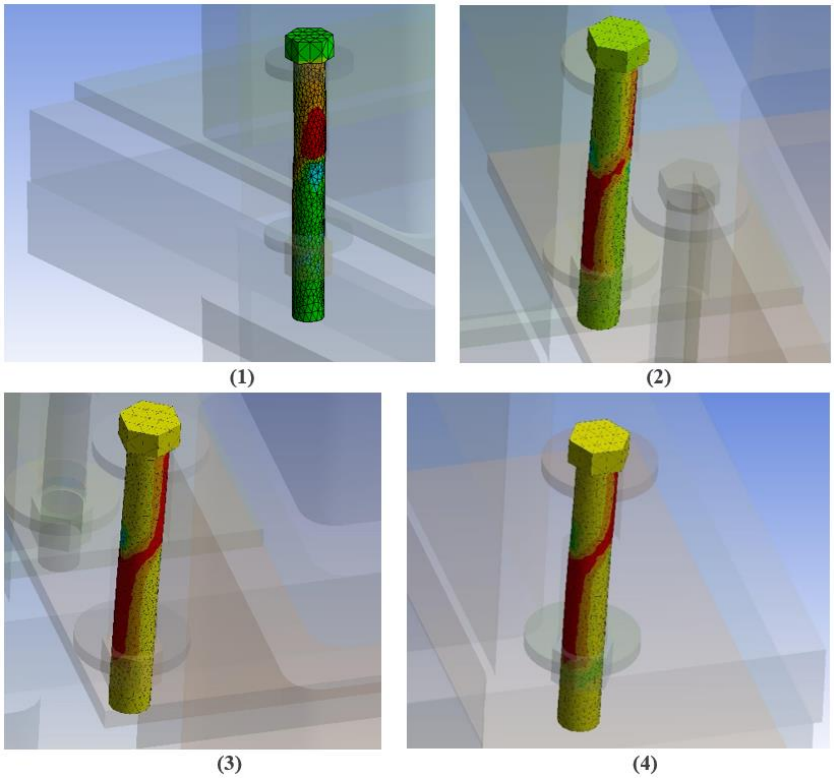

Figure 26: Bolt (1-4) failure mode of connection C1.

5.2. Estimating the Stiffness of the Connection

The accurate estimation of connection stiffness can help in global modelling of MBSs, where these values can be used as an equivalent spring stiffness for connection points represented as either link or spring type elements. Only the elastic stiffness of the connection was considered here, as the main intention is to identify the stiffness value for the final connection design. Stiffness was calculated for both the initial slip and the shear deformation, which are the 2 distinct stages of bolt connection deformation observed. Bolts 1-4, a combination of springs connected stiffness, were separately estimated and combined as in the resistance arrangement shown in Figure 27.

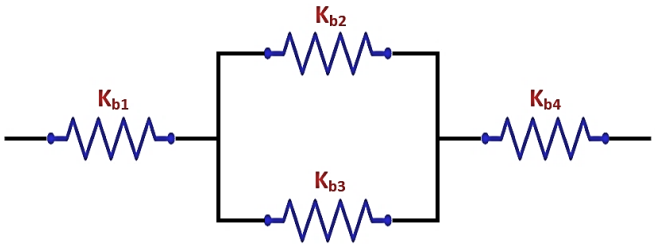

Figure 27: Representation of overall connection stiffness as a combination of individual bolt stiffness.

The resultant stiffness can be calculated from Eq. (6), where the 2 bolts in the middle (b2 and b3) are considered parallel, and their combined stiffness will act in series with corner bolts b1 and b4.

$$\frac{1}{k} = \frac{1}{k_{b1}} + \frac{1}{(k_{b2}+k_{b3})} + \frac{1}{k_{b4}} \quad (6)$$

5.2.1. Slip Stiffness (k_{slip})

The shear slip stiffness for every individual bolt was calculated based on Eq. (7). Where, k_{slip} is stiffness against the initial slip; P_{slip} is the load applied during the initial slip; Δ_{slip} is initial slip value (slip to the bolt hole edge tolerance). The overall stiffness value for the entire connection was then calculated using Eq. (6).

$$k_{slip} = {}^{P_{slip}}\!/_{\Delta_{slip}} \quad (7)$$

5.2.2. Stiffness against combined Shear and Tension (k_{br})

Based on Hooke's law, the stiffness against shear (k_τ) can be estimated using Eq. (9) [30]. According to Wileman et al. [31], the connection stiffness against tension (k_m) is estimated though an exponential relationship as per Eq. (9). And then the combined shear and tension stiffness of the entire connection therefore can be expressed as in Eq. (10).

$$k_\tau = {}^{GA_s}\!/_{L} \quad (8)$$

$$k_m = AEde^{B\left(\frac{d}{L}\right)} \quad (9)$$

$$\frac{1}{k_{br}} = \frac{1}{k_\tau} + \frac{1}{k_m} \quad (10)$$

Where G is the shear modulus of the material; A_s is bolt cross-sectional area; L is grip length of bolt; A , B are the dimensional constants which carries values of 0.78715 and 0.62873 respectively for steel; E is elasticity modulus of material; d is diameter of bolt hole. Similar to slip stiffness, each plate in a connection linked by a single bolt has its stiffness computed independently and then combined in series.

The summary of design capacities of connections C1, C2 and C3, where the theoretical stiffness values obtained were compared with analytical and experimental results, is provided in Table 5. In addition, the analytical and experimental stiffness were evaluated based on analyzing a typical portion from the elastic zone of the load - deformation curve.

Table 5: Design capacities of connections C1-C3.

Connection Design	Theoretical connection stiffness (kN/mm)	Analytical connection stiffness – from ANSYS model (kN/mm)	Experimental connection stiffness (kN/mm)
C1	74.9	102.6	137.9
C2	134.9	148.4	225.0
C3	134.9	152.0	285.0

The stiffness of connection derived from analytical model shows a closer match with theoretical calculations than those of experimental results. This could be due to the fact that numerical models are more controlled simulations with theorised parameters, where in case of experiments, laboratory investigations are dependent on a large number of factors that can diverge from expected values. Deviations in thickness of clamping plates, size of the bolt holes and loss of applied preload during the experiments are factors which may possibly have influenced the variation of these stiffness values.

6. Conclusions

In MBSs, the intermodular connections are crucial in transferring and resisting lateral loads. The lateral loads are transferred from horizontal elements to stiffer vertical members via these connections that link neighbouring modules. Hence, a better knowledge of their behaviour when subjected to lateral loads is essential. In this study, experiments were performed on 3 distinctive connection configurations to successfully validate the FEMs. The experiments and verified models along with theoretical design calculations, provided a great insight into how the connection would respond to horizontal stresses. Based on that, the following conclusions were drawn.

1. Comparison of load-deformation responses of the experiment and the FEMs indicated a close agreement, especially in the initial slip stage. And in addition, the experimental and finite element model slip resistances of the connections have given a test to model output slip resistance ratio of 1.03-1.07 for connection C1-C3 with an average of 1.04, showing an acceptable accuracy providing research basis for further investigations.
2. The detailed analyses on all 3 connection configurations reveal that, the connection tends to fail in slippage even at a very small lateral load. Therefore, the proposed connection should be considered a ‘slip critical’ connection when designed for serviceability.
3. Shear stress-strain curves exhibited a gradient of 76.9 GPa equal to the shear modulus of the material, which also indicates that the pure shear is not the most critical failure criteria. However, further evaluation of combined tension and shear effects on the connections confirmed that the failures were due to the combined effect, and therefore connections of this type should consider this as the most critical design check.
4. Finally, the stiffness capacities of the connection designs C1-C3 was acquired as 102.6, 148.4, and 152.0 kN/mm respectively, from finite element analysis showing a closer match with theoretical calculation outputs. Hence, the obtained stiffness values can be adopted in the global structural model of MBSs, where connection can be modelled as either link or spring type element.

Following are suggestions and recommendations for further investigations based on the understanding developed from this study.

1. Slip failure is unavoidable for large horizontal stresses, such as those experienced during seismic events. As a result, bolt slippage should be expected during an earthquake. Even though slip failure is not catastrophic, it does convert the connection to a bearing type connection. Hence, as in C3 design, wider slots are not recommended for high rise modular buildings because cumulative slips can generate a substantial lateral deflection and can cause damage to supporting elements.
2. Slotted holes are very appealing for modular construction because they provide a higher tolerance margin when aligning the top modules with the bolt holes of the fixed bottom modules. If slotted holes are still necessary to favour installation, they must be appropriately engineered to prevent slippage. This can be accomplished by using larger bolt sizes than that are required. This approach, however, is not recommended in seismically active regions.
3. Another option for satisfying this requirement during module installation is to employ specialised technologies for example specially designed interlock or self-lock connections, to support the module while it is precisely positioned for installation. This would help considerably reduce human errors and offer a safer working environment during module installation while also allowing for the installation of modules with considerably lower tolerances.

References

[1] S. Navaratnam, T. Ngo, T. Gunawardena, and D. Henderson, "Performance review of prefabricated building systems and future research in Australia," *Buildings*, vol. 9, no. 2, pp. 1–13, 2019, doi: 10.3390/buildings9020038.

[2] Y. Wang, J. Xia, R. Ma, B. Xu, and T. Wang, "Experimental Study on the Flexural Behavior of an Innovative Modular Steel Building Connection with Installed Bolts in the Columns," *Appl. Sci.*, vol. 9, no. 17, p. 3468, 2019, doi: 10.3390/app9173468.

[3] T. Gunawardena, P. Mendis, T. Ngo, B. Rismanchi, and L. Aye, "Effective use of offsite manufacturing for public infrastructure projects in Australia," *Int. Conf. Smart Infrastruct. Constr. 2019, (ICSIC 2019)*, pp. 267–273, 2019, doi: 10.1680/icsic.64669.267.

[4] E. F. Deng, J. B. Yan, Y. Ding, L. Zong, Z. X. Li, and X. M. Dai, "Analytical and numerical studies on steel columns with novel connections in modular construction," *Int. J. Steel Struct.*, vol. 17, no. 4, pp. 1613–1626, 2017, doi: 10.1007/s13296-017-1226-5.

[5] H. Rajanayagam *et al.*, "A-State-Of-The-Art review on modular building connections," *Structures*, vol. 34, pp. 1903–1922, 2021, doi: 10.1016/j.istruc.2021.08.114.

[6] J. Hwan Doh, N. M. Ho, D. Miller, T. Peters, D. Carlson, and P. Lai, "Steel Bracket Connection on Modular Buildings," *J. Steel Struct. Constr.*, vol. 02, no. 02, 2017, doi:

10.4172/2472-0437.1000121.

[7] T. Gunawardena and P. Mendis, "Prefabricated Building Systems — Design and Construction," *Encyclopedia*, pp. 70–95, 2022, doi: http://dx.doi.org/10.3390/encyclopedia2010006.

[8] R. M. Lawson and R. G. Ogden, "Sustainability and Process Benefits of Modular Construction," *18th CIB World Build. Congr.*, pp. 38–51, 2010, [Online]. Available: https://www.irbnet.de/daten/iconda/CIB18783.pdf.

[9] P. Sharafi, M. Mortazavi, B. Samali, and H. Ronagh, "Interlocking system for enhancing the integrity of multi-storey modular buildings," *Autom. Constr.*, vol. 85, pp. 263–272, 2018, doi: 10.1016/j.autcon.2017.10.023.

[10] S. Shan and W. Pan, "The structural performance of high-rise buildings with steel modules is closely related to the mechanical behaviors of structural connections," *Struct. Des. Tall Spec. Build.*, vol. 29, no. 15, pp. 1–20, 2020, doi: 10.1002/tal.1788.

[11] T. Gunawardena, T. Ngo, P. Mendis, and J. Alfano, "Innovative Flexible Structural System Using Prefabricated Modules," *J. Archit. Eng.*, vol. 22, no. 4, 2016, doi: 10.1061/(asce)ae.1943-5568.0000214.

[12] T. Gunawardena, T. Ngo, and P. Mendis, "Behaviour of multi-storey prefabricated modular buildings under seismic loads," *Earthq. Struct.*, vol. 11, no. 6, pp. 1061–1076, 2016, doi: 10.12989/eas.2016.11.6.1061.

[13] J. Peng, C. Hou, and L. Shen, "Lateral resistance of multi-story modular buildings using tenon-connected inter-module connections," *J. Constr. Steel Res.*, vol. 177, p. 106453, 2021, doi: 10.1016/j.jcsr.2020.106453.

[14] A. W. Lacey, W. Chen, H. Hao, and K. Bi, "Review of bolted inter-module connections in modular steel buildings," *J. Build. Eng.*, vol. 23, pp. 207–219, 2019, doi: 10.1016/j.jobe.2019.01.035.

[15] C. D. Annan, M. A. Youssef, and M. H. El Naggar, "Seismic overstrength in braced drames of modular steel buildings," *J. Earthq. Eng.*, vol. 13, no. 1, pp. 1–21, 2008, doi: 10.1080/13632460802212576.

[16] R. M. Lawson and J. Richards, "Modular design for high-rise buildings," *Proc. Inst. Civ. Eng. Struct. Build.*, vol. 163, no. 3, pp. 151–164, 2010, doi: 10.1680/stbu.2010.163.3.151.

[17] C. D. Annan, M. A. Youssef, and M. H. Ei-Naggar, "Effect of directly welded stringer-to-beam connections on the analysis and design of modular steel building floors," *Adv. Struct. Eng.*, vol. 12, no. 3, pp. 373–383, 2009, doi: 10.1260/136943309788708400.

[18] M. T. Gorgolewski, P. J. Grubb, and M. Lawson, *Modular Construction using Light Steel Framing - Design of Residential Buildings*, P302 ed. Berkshire: The Steel Construction Institute, 2001.

[19] A. J. Styles, F. J. Luo, Y. Bai, and J. B. Murray-Parkes, "Effects of joint rotational stiffness on structural responses of multi-story modular buildings," in *Transforming the Future of Infrastructure through Smarter Information - Proceedings of the International Conference on Smart Infrastructure and Construction*, 2016, pp. 457–462, doi: 10.1680/tfitsi.61279.457.

[20] R. M. Lawson, R. G. Ogden, and R. Bergin, "Application of Modular Construction in High-Rise Buildings," *J. Archit. Eng.*, vol. 18, no. 2, pp. 148–154, 2012, doi: 10.1061/(asce)ae.1943-5568.0000057.

[21] J. F. Zhang *et al.*, "Component method based rotation performance and design method for the connection in ATLS modular house," *Thin-Walled Struct.*, vol. 164, no. April, p. 107803, 2021, doi: 10.1016/j.tws.2021.107803.

[22] P. C. Kohnke, "ANSYS," in *Finite Element Systems*, 1982.

[23] ARAMIS, "ARAMIS User Information - Hardware." Gesellschaft für Optische Messtechnik (GOM), Germany, 2008.

[24] *Australia S. AS 4100:2020 Steel Structures*. Standards Australia, 2020.

[25] B. E. Gorenc, R. Tinyou, and A. Syam, *Steel Designers Handbook*. Sydney, Australia: University of New South Wales Press, 2005.

[26] AJAX, *Fastener Handbook: Bolt Products*. AJAX Technical Advice Centre (ATAC), 1999.

[27] T. Gunawardena, "Behaviour of Prefabricated Modular Buildings Subjected to Lateral Loads (Thesis)," The University of Melbourne, 2016.

[28] B. E. Gorenc, R. Tinyou, and A. Syam, *Steel Designers Handbook*. Sydney, Australia: University of New South Wales Press, 2005.

[29] G. L. Kulak, J. W. Fisher, and J. H. A. Struik, *Guide to Design Criteria for Bolted and Riveted Joints Second Edition*. Chicago, USA: John Wiley & Sons, 1991.

[30] VanGaasbeek C. J., "Numerical Modeling of Bolted Joints. An Applied Finite Element Analysis Approach (Masters Thesis)," Polytechnic Institute, Connecticut, USA, 2011.

[31] J. Wileman, M. Choudhury, and I. Green, "Computation of member stiffness in bolted connections," *J. Mech. Des. Trans. ASME*, vol. 113, no. 4, pp. 432–437, 1991, doi: 10.1115/1.2912801.